International Journal of the Physical Sciences Vol. 6(33), pp. 7420 - 7427, 9 December, 2011
Available online at http://www.academicjournals.org/IJPS
ISSN 1992 - 1950 ©2011 Academic Journals

Full Length Research Paper

Thermodynamic treatment in a case of heavy ion collision

M. M. Aesh[1]*, S. M. Maise[1], H. M. EL Samman[1] and M. T. Hussein[2]

[1]Physics Department, Faculty of Science, Minoufia University, Sheben El-Koom, Egypt.
[2]Physics Department, Faculty of Science, Cairo University, 12613 Giza, Egypt.

Accepted 1 July, 2011

The strong interaction described by quantum chromodynamics may be studied under conditions of high parton temperature and high energy density, using relativistic heavy ion collisions. High energy heavy ion collisions aim to recreate the conditions which existed a few microseconds following the big bang, and determine the properties of this super-dense matter. The density of produced hadrons is very high, at energy densities of 200(130) GeV/fm3. The quark-gluon plasma produced at high temperature and high energy density studies thermodynamic model for heavy ion collision at different energies. One of the main objective of thermodynamic model is to observe the quantum chromodynamics phase transition of hadron matter to quark-gluon plasma. Central collisions of two gold nuclei at the top energy of the relativistic heavy ion collider (RHIC) at Brookhaven National Laboratory produced thousands of charged particles. These are the largest particle multiplicities generated in man-made subatomic reactions. The hope is that these complex systems may reveal evidence of the creation and decay of a quark-gluon plasma, where quarks and gluons are allowed to explore a volume larger than that of typical hadrons.

Key words: Quark-gluon plasma, quantum chromodynamics, relativistic heavy ion collider, ion.

INTRODUCTION

One of the most remarkable results to emerge from relativistic heavy-ion collisions over the past years is the striking regularity shown by particle yields at all beam energies. From the lowest silicon integrated system (SIS) up to the highest RHIC energies, all results on particle multiplicities are consistent with the assumption of chemical equilibrium in the final-state fireball produced after heavy-ion impact (Braun et al., 2004). The particle yields are found to be described, with remarkable precision, by a thermal-statistical model that assumes approximate chemical equilibrium (Braun-Munzinger et al., 2004; Cleymans and Satz, 1993; Becattini et al., 2001; Braun-Munzinger et al., 1995; Braun-Munzinger et al., 1999; Cleymans et al., 2005; Braun-Munzinger et al., 2002; Becattini et al., 2004; Cleymans et al., 1999; Becattini et al., 2001; Averbeck et al., 2003; Kraus, 2005; Broniowski et al., 2002; Baran et al., 2004). For a given Bravina et al., 2002; By STAR Collaboration, 2005; collision energy, the thermal-statistical model with only two parameters, the temperature (T) and baryon chemical potential (μB), provides a very systematic description of particle yields.

In the next few years, the BNL-RHIC (Au-Au collisions at √s=200 GeV per incident nucleon pair) and the CERN-LHC (Pb-Pb collisions at √s = 5.5 A TeV) accelerators will provide the opportunity to study a new phase of matter, namely the so-called quark-gluon plasma (QGP) (Proceedings of 14th International Conference, 1999).

The evolution of the QGP towards (local) equilibrium can be studied by solving transport equations for quarks and gluons with all the dynamical effects taken into account. Obviously, the first problem one always encounters is the correct computation of the initial conditions needed to solve the transport equation. This is because one cannot calculate the parton production in all range of momentum from perturbative QCD (pQCD). There are also coherence effects (McLerran and

*Corresponding author. E-mail: mohamedeash2@yahoo.com.

Abbreviations: RHIC, relativistic heavy ion collider; **QGP,** quark-gluon plasma.

Venugopalan, 1994; Kovchegov and Mueller, 1998) that play an important role in the early stage of the nuclear collision at very high energy. For small x and large nuclei, the QCD based calculation performed by Kovner et al. (1998) predicts the existence of a coherent field in a certain kinematical range. That field may play an important role in the equilibration of the plasma.

THE THERMODYNAMIC MODEL

Let us consider the collision between a target nucleus T and a projectile P at a given impact parameter b, the collision goes through sequential stages. The first is a compression of the nuclear matter due to the high energy interaction, forming a fireball with diffusive surface, contrary to standard fireball model assumptions (Hussein et al., 2000; Gosset et al., 1977) which support the concept of participant and spectator nucleons with pure cylindrical cut in the nuclear matter. The nuclear matter is then treated as a heterogeneous thermodynamic system. Multiple nuclear collisions occur inside the fireball, increasing the energy density and allowing the formation of quark gluon plasma state. This leads to creation of new particles and expands the system which gradually approaches the equilibrium state.

The last stage is the fireball decay. Particle emission from the fireball is allowed at diffuseness points on the time scale of the reaction. Light created particles are expected to be emitted on the early stage in a narrow forward cone angle, due to the first few collisions. The higher order collisions draw the system towards the equilibrium state producing particles in isotropic distribution in phase space. It is then convenient to consider the state of equilibrium as a time reference for the reaction. Drawing back, we may follow the historical growth of particle emissions on the time scale. Hadronic matter inside the fireball is partially formed by the fast projectile nucleons and the slow target ones. The relative projectile density in this mixture is a very important parameter. It determines the thermodynamic parameters, the center of mass velocity, the temperature and the temperature gradient inside the fireball matter. We use a Gaussian density distribution (Cleymans et al., 1999) for nuclei of mass number $A< 20$, while a Fermi density for $A\geq 20$. Consider a frame of reference which coincides with the center of the target nucleus in the laboratory system. Then the relative projectile density $\rho(r, b)$, at a given distance r inside the fireball matter and a given impact parameter b is given by:

$$\eta(r,b) = \frac{\rho_p(r-b)}{\rho_p(r-b) + \rho_T(r+b)} \quad (1)$$

We use Woods-Saxon distribution. Here we adopt the Woods-Saxon formalism, as this is widely used to characterize measurements of the radial density of charged nucleons in a nucleus. The Woods-Saxon distribution is given by:

$$\rho(r) = \frac{\rho_0(1 + wr^2/R^2)}{1 + \exp((r-R)/a)} \quad (2)$$

Where, r is the radial distance from the center of the nucleus; R, mean radius of the nucleus; a, "skindepth" of the nucleus; ρ_o, nuclear density constant; W=0.0, Au nucleus.

The center of mass energy

$$\xi_{cm} = 3T + m\frac{k_1(m/T)}{k_2(m/T)} \quad (3)$$

Where,

$$\xi_{cm} = (M_T^2 + M_P^2 + 2M_T E_P)^{1/2} = (N_T^2 M^2 + N_P^2 M^2 + 2N_T M N_P t_i)^2$$

The average value of the center of mass energy

$$\bar{\xi}_{cm} = \frac{\xi_{cm}}{N_T + N_P} = \left(M^2 \left(\frac{N_T^2 + N_P^2}{(N_P + N_T)^2} \right) + 2Mt_i \left(\frac{N_T N_P}{(N_P + N_T)^2} \right) \right)$$

$$\bar{\xi}_{cm} = \left[m^2 + 2mt_i \eta(1-\eta) \right]^{1/2}$$

Local temperature T (r) at a position vector; r is the solution of the thermodynamic energy conservation.

$$\left[m^2 + 2\eta(1-\eta) mt_i \right]^{1/2} = 3T + m\frac{K_1(m/T)}{K_2(m/T)} \quad (4)$$

From Equation 4 one can find $T=\lambda\eta(1-\eta)$

Where, λ, constant; m, rest mass of the constituent particle of the nuclear medium under investigation; *K1, K2*, McDonalds functions of first and second order (Hegab et al., 1990); t_i, incident kinetic energy per nucleon.

Equation 4 is valid for each type of particles forming the fireball. The temperature is very sensitive to the form of the nuclear density. The momentum distribution of the fireball nucleons in the center of mass system is given by the following relation:

$$\frac{d^2N}{p^2 dp d\Omega} = \frac{N}{4\pi m^3} \frac{\exp(-E/T)}{2(T/m)^2 K_1(m/T) + (T/m) K_1(m/T)} \quad (5)$$

The equilibrium energy distribution in the laboratory system is given by

$$f_o(E,r) = PE^o \frac{d^2N}{P^2 dP d\Omega} \quad (6)$$

The prime letters are defined in the center of mass system

and relativistically transformed as:

$$E^0 = \gamma_{cm}(E_L - \beta_{cm} P_L \cos\theta_L) \quad (7)$$

Where the center of mass velocity β_{cm} is given by:

$$\beta_{cm}\frac{P_L}{E_L} = \frac{\eta[t_i(t_i+2m)]^{1/2}}{m+\eta t_i} \quad (8)$$

And γ_{cm} is given by:

$$\gamma_{cm} = \frac{1}{\sqrt{1-\beta^2}}$$

Since particles emission is allowed before approaching the equilibrium state, and then it is convenient to use the Vlasov equation 7 to deal with the particle energy spectra at any time of the reaction. The Vlasov equation has the form.

$$\frac{df}{dt} = \frac{\partial f}{\partial t} + \frac{P}{m}\nabla_r U \nabla_p f \quad (9)$$

Where, *r* is the scalar potential acting among the particles.

Equation 9 may be solved under some approximations. First, we shall consider a pre-equilibrium state where the time derivative $^{df/dt}$ may be approximated as

$(f - f0)/tc$

Where, *fo* is the equilibrium distribution.

Since we are dealing with a state near equilibrium, so it is convenient to consider the rate of change of the function f approximately equal to that of f_o. So we replace f by f_o in the right hand side (RHS) of Equation 9. Moreover, let us consider the particles as almost free so that we neglect the potential U in this stage of approximation. Equation 9 then becomes,

$$f1 = f_0 + t_c\frac{P}{m}\nabla_r f_0 = f_0 + t_c\frac{P}{m}\cos\theta\frac{\partial f_0}{\partial r} \quad (10)$$

Where, f_1, first order approximation of the particle spectrum; tc, time interval required by the system to approach the equilibrium state; fo and θ, scattering angle, the angle between the direction of particle emission P and the radial direction r.

A second order approximation is obtained by using f1 instead of f in the RHS of Equation 9, so that,

$$f_2 = f_0 + t_c\frac{P}{m}\cos\frac{\partial f_0}{\partial t} + (t_c\frac{P}{m}\cos\theta)^2\frac{\partial^2 f_0}{\partial r^2} \quad (11)$$

By the same analogy we get the recursion relation for the nth order approximation as;

$$f_n = f_0 + \sum_{t=1}^{n}\left(t_c\frac{P}{m}\cos\theta\right)^t\frac{\partial^t f_0}{\partial r^t} \quad (12)$$

so that the third and fourth order approximations are;

$$f_3 = f_2 + \left(t_c\frac{P}{m}\cos\theta\right)^3\frac{\partial^3 f_0}{\partial r^3} \quad (13)$$

$$f_4 = f_3 + \left(t_c\frac{P}{m}\cos\theta\right)^4\frac{\partial^4 f_0}{\partial r^4} \quad (14)$$

RESULTS AND DISCUSSION

The predictions of the pre equilibrium model were applied to the P^1+P^1, S^{32}+O^{16}, Au^{197}+Au^{197} and Ne^{20}+U^{238} collisions at 20 and 130 A GeV. Assuming a frame of reference coincides with the center of the target, and that the projectile is located at a position r, with an impact parameter b. The relative projectile density η(r, b) is calculated according to Equation 1. In Figure 1, we demonstrate η (r, b) averaged over the whole range of impact parameter. The function η (r, b) shows a peak value of a height at a different distance, where the projectile and the target have equal densities. According to the model assumptions, the nuclei have no sharp surface density but instead, a diffuseness surface which extends the range of the nuclear matter to about twice the sum of the nuclear radii. On the other hand, the geometrical factor represented by the size of the nuclear matter has heavy weight near the origin and falls exponentially with r toward the surface as may be described by the tail of the Gaussian distribution. In Figure 2, the temperature shows a peak depending on the target nucleus, the distance increases from Proton to Uranium, tail seen in O^{16}+S^{32} collision. The effective range, where the nuclear matter forming the nuclear thermodynamic system has appreciable value depends on the target nucleus. The parameter η has a main role in evaluating the temperature and its gradient inside the nuclear matter as seen by Equation 2. Figure 3 shows the temperature as a function of η for the reactions at 20 and 130 GeV incident kinetic energy per nucleon. The maximum temperature is found to be 250 MeV. The proton density function in its equilibrium form is calculated according to Equation 6 over the effective range of the thermodynamic system. Figure 7 shows zero order term of vlassov equation and the differentiation of first order. The results are shown in Figure 8,11,12,13 and 14 for protons emitted with EL = 30, 120 and 180 MeV

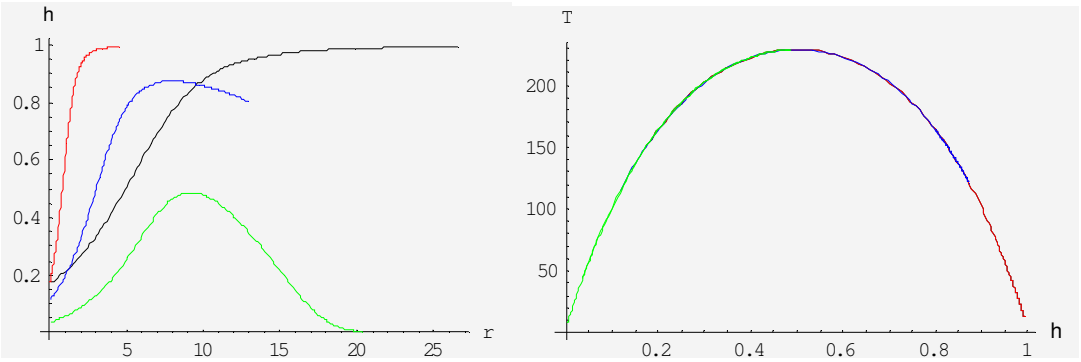

Figure 1. Relation between relative projectile density η (r) and radial distance for P^1+P^1 collision. Where, red (doted), $S^{32}+O^{16}$collision; blue (dashed), $Au^{197}+Au^{197}$ collision; Black (Solid)& $Ne^{20}+U^{238}$ collision Green.

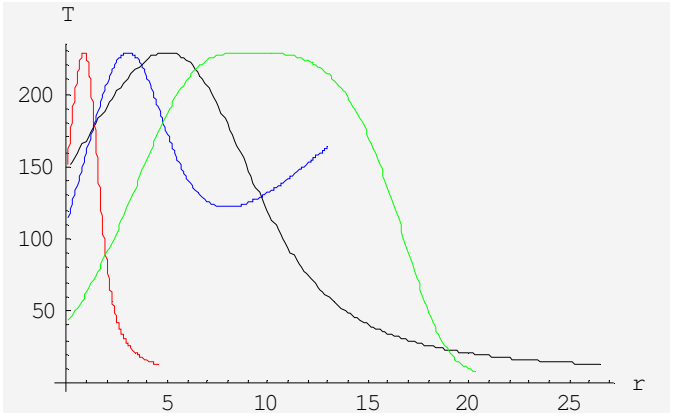

Figure 2. Relation between temperature (T) and radial distance for P1+P1 collision. Where, red (doted), S32+O16 collision; blue (dashed), Au197+Au197collision; Black (Solid) and Ne20+U238collision Green.

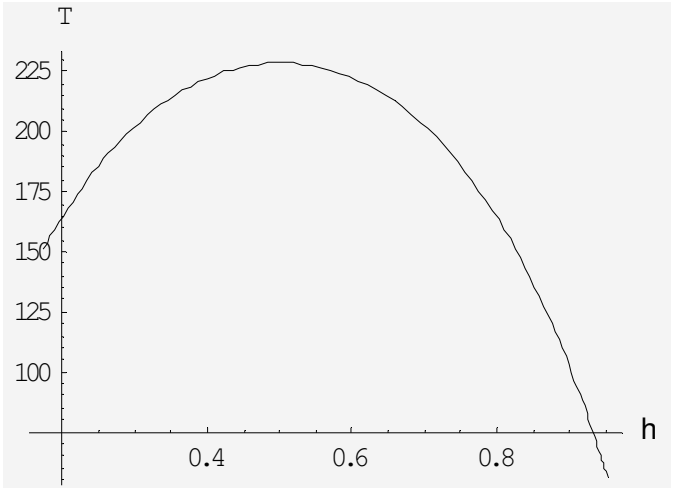

Figure 4. Relation between temperature and nuclear density for $Au^{197}+Au^{197}$at 20GeV.

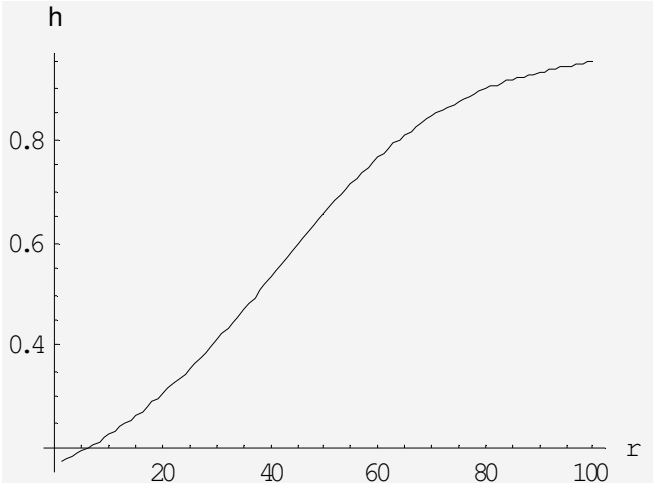

Figure 3. Relation between nuclear density and radial distance for $Au^{197}+Au^{197}$at 20GeV.

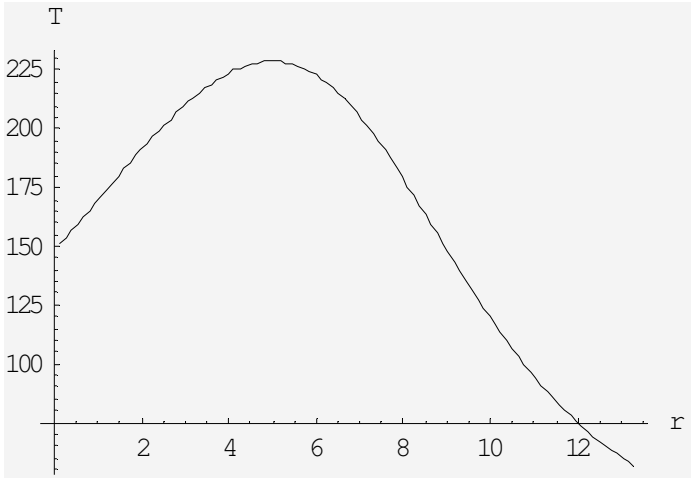

Figure 5. Relation between temperature and radial distance for $Au^{197}+Au^{197}$at 20GeV.

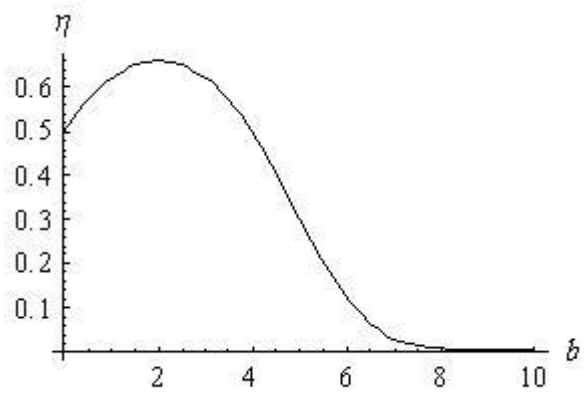

Figure 6. Relation between nuclear density with impact parameter joined for Au^{197}+Au^{197}at 20GeV.

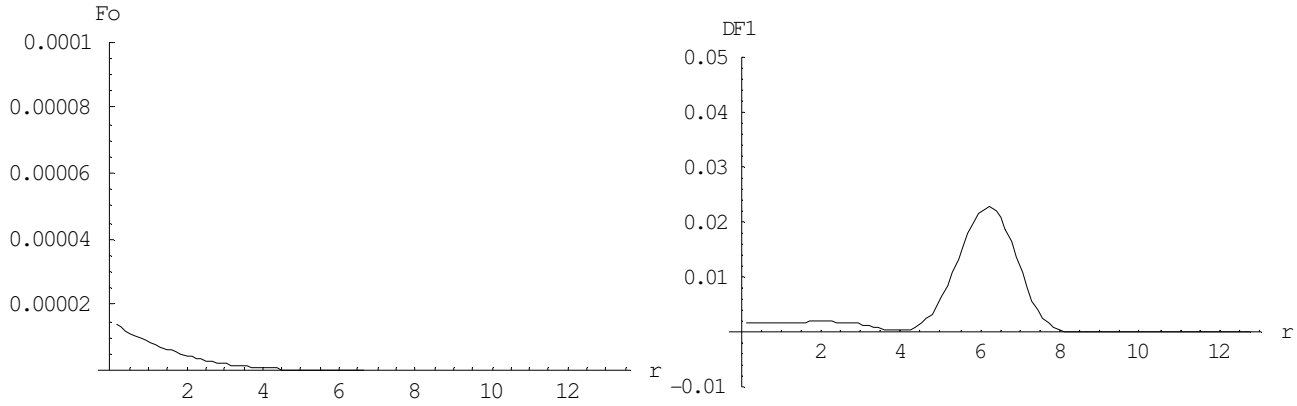

Figure 7. Zero order term of Vlasov equation and the differentiation of first order.

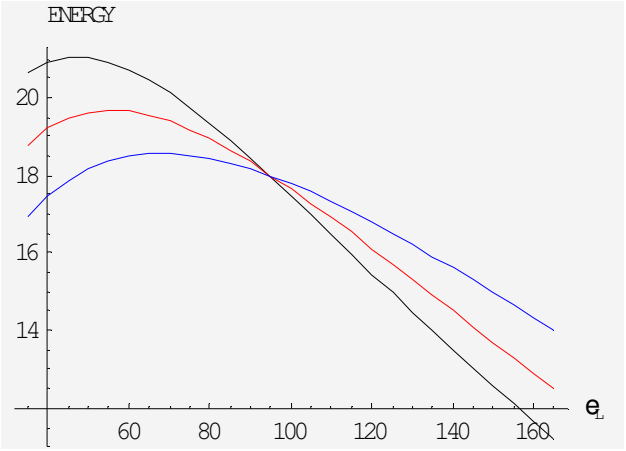

Figure 8. The energy spectra of protons produced for Au^{197}+Au^{197}interactions at 20 A GeV, at emission angle 90°. First correction term, black, second correction term, red and third correction term, blue with an emission time parameter t = –5.5 $(GeV)^{-1}$.

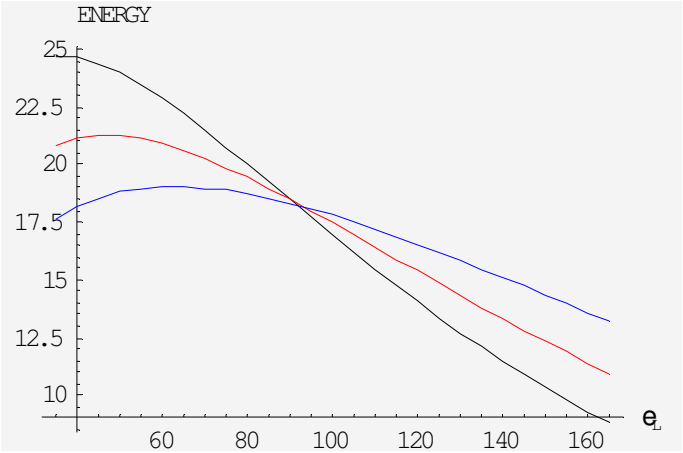

Figure 9. The energy spectra of Kions produced for Au^{197}+Au^{197}interactions at 20 A GeV, at emission angle 90°. First correction term, black, second correction term, red and third correction term, blue with an emission time parameter t = –5.5 $(GeV)^{-1}$.

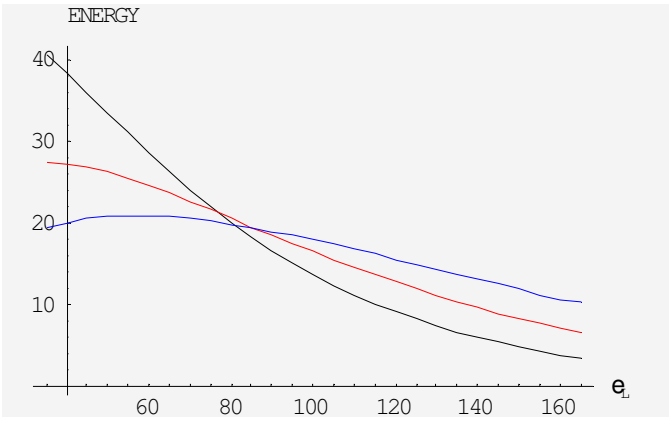

Figure 10. The energy spectra of pions produced for $Au^{197}+Au^{197}$ interactions at 20 A GeV, at emission angle 90°. First correction term, black, second correction term, red and third correction term, blue with an emission time parameter t = –5.5 $(GeV)^{-1}$.

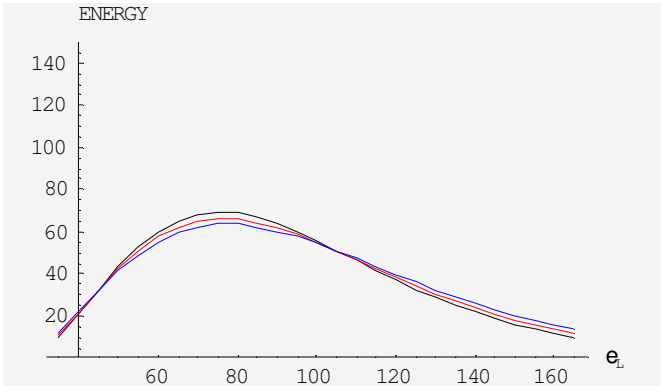

Figure 13. The energy spectra of protons produced for $Au^{197}+Au^{197}$interactions at 130 A GeV, at emission angle of 60 and 90°. First correction term, black, second correction term, red and third correction term, blue with an emission time parameter t = –5.5 $(GeV)^{-1}$.

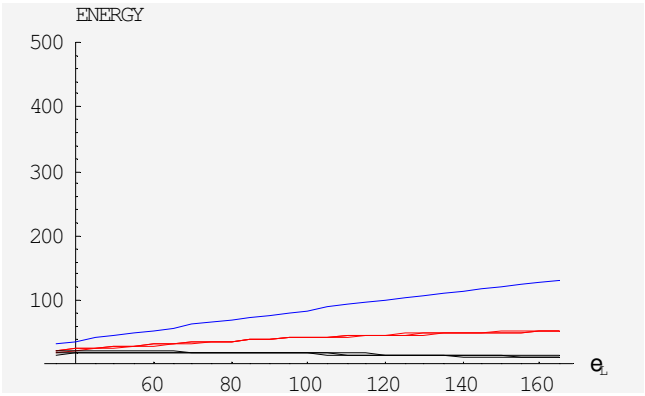

Figure 11. The second order corrected pre-equilibrium energy spectra of protons produced for $Au^{197}+Au^{197}$interactions at 20 A GeV, at emission angles of 30 blue, 60 red and 90 black.

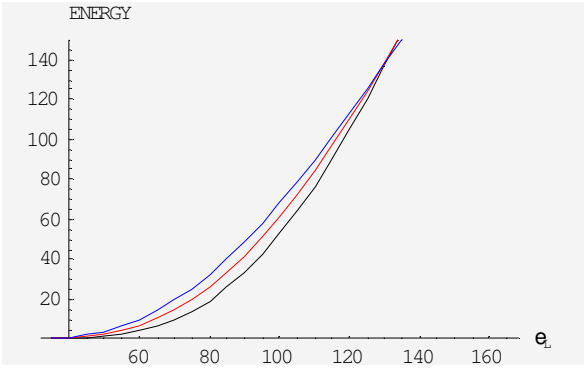

Figure 14. The energy spectra of protons produced for $Au^{197}+Au^{197}$interactions at 130 A GeV , at emission angle 30 and 90°. First correction term, blue, second correction term, red and third correction term, black with an emission time parameter t = –5.5 $(GeV)^{-1}$.

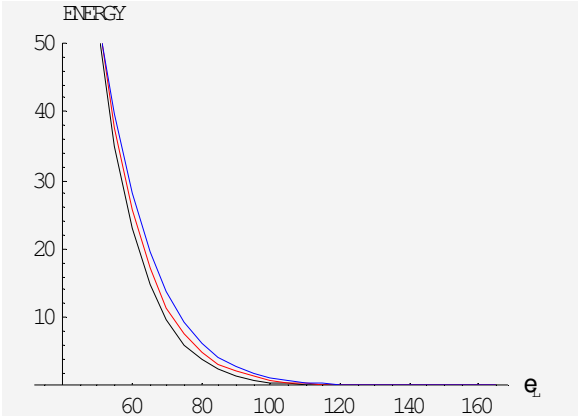

Figure 12. The energy spectra of protons produced for $Au^{197}+Au^{197}$interactions at 130 A GeV, at emission angle of 90°. First correction term, blue, second correction term, red and third correction term, black with an emission time parameter t = –5.5 $(GeV)^{-1}$.

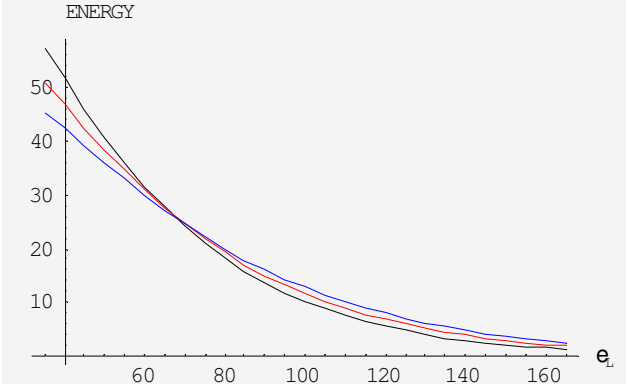

Figure 15. The energy spectra of Kions produced for $Au^{197}+Au^{197}$interactions at 130 A GeV, at emission angle of 90°. First correction term, black, second correction term, red and third correction term, blue with an emission time parameter t = –5.5 $(GeV)^{-1}$.

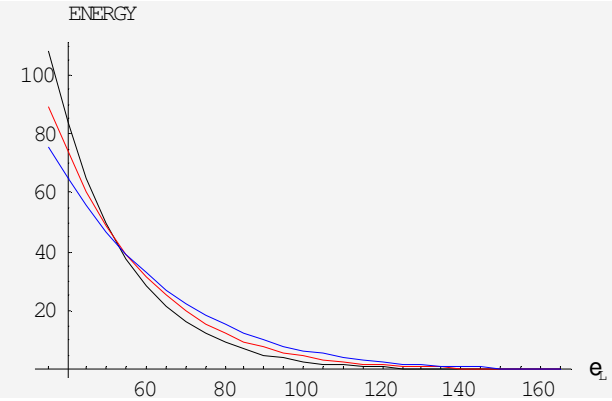

Figure 16. The energy spectra of pions produced for $Au^{197}+Au^{197}$interactions at 130 A GeV, at emission angle 90^0. First correction term, black, second correction term, red and third correction term blue with an emission time parameter t = –5.5 $(GeV)^{-1}$.

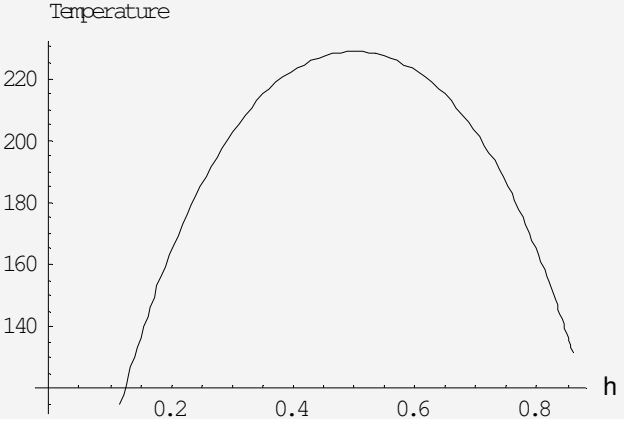

Figure 17. Relation between temperature and energy density for $S^{32}+O^1$

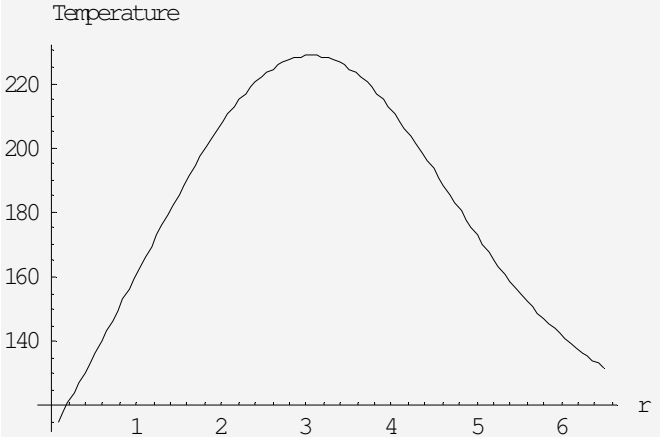

Figure 18. Relation between temperature and radial distance for $S^{32}+O^{16}$

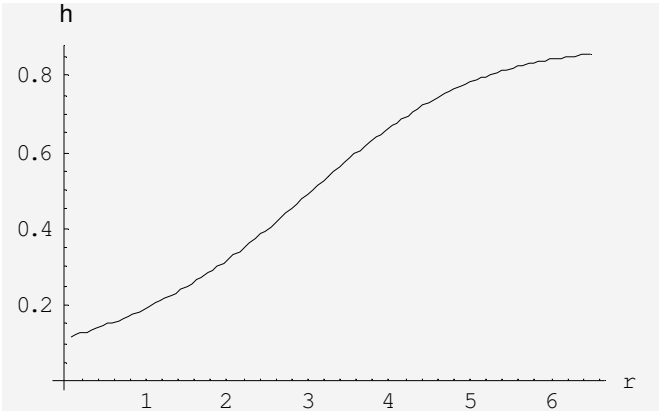

Figure 19. Relation between nuclear density with radial distance for $S^{32}+O^{16}$.

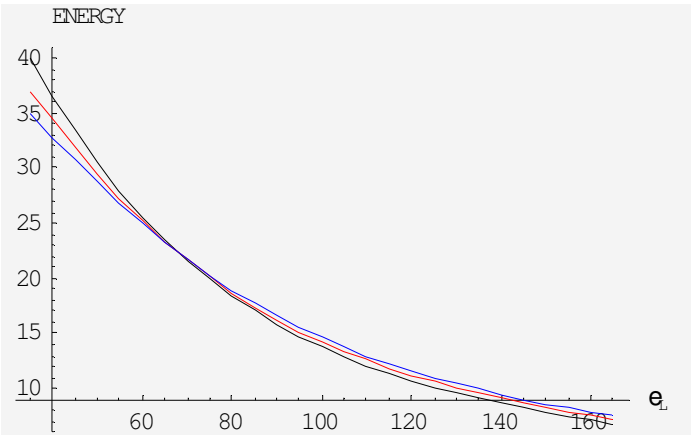

Figure 20. The energy spectra of protons produced for $S^{32}+O^{16}$ interactions at 1 A MeV, at emission angle 90°. First correction term, black, second correction term, red and third correction term, blue with an emission time parameter t = –5.5 $(GeV)^{-1}$.

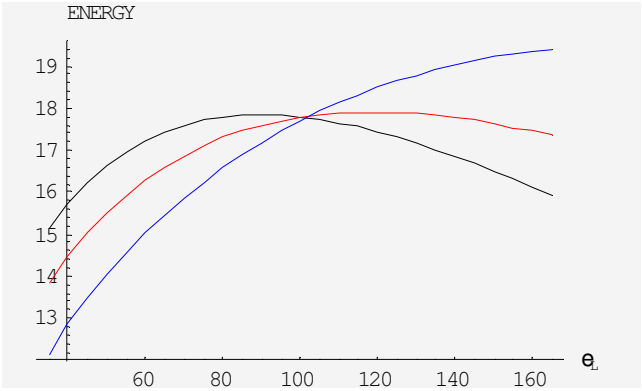

Figure 21. The energy spectra of protons produced for $S^{32}+O^{16}$ interactions at 2100A MeV, at emission angle 90°. First correction term, black, second correction term, red and third correction term, blue with an emission time parameter t = –5.5 $(GeV)^{-1}$.

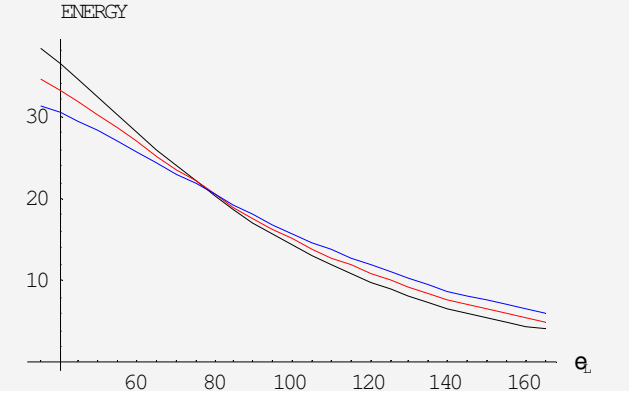

Figure 22. The energy spectra of protons produced for $S^{32}+O^{16}$ interactions at 100A GeV, at emission angle 90^0. First correction term, black, second correction term, red and third correction term, blue with an emission time parameter t = –5.5 $(GeV)^{-1}$.

with emission Lab angle of 30, 60 and 90°. The protons produced at low energy show anisotropic distribution with peaks near the origin and the surface of the thermodynamic system. The position of the two peaks corresponds to the regions characterized by low η values and consequently low temperature; the bulk of which corresponds to high temperature zones. The yield from the low temperature zones decreases with increase in the energy of the emitted protons. The spatial variation of the function f_o (r, p) is also studied.

CONCLUSION

We studied thermodynamic model of heavy ion collision at high energy and compared it with medium and low energy for different collision. The thermodynamic model studied the nucleus-nucleus collisions and some thermodynamic variables, The thermodynamic model was able to solve Vlasov equation. The results from this model for P1+P1 collision, S32+O16 collision, Au197+Au197 collision and Ne20+U238 collision at different energies used the Fire ball model.

REFERENCES

Averbeck R, Holzmann R, Metag V, Simon RS (2003). Neutral Pions and Eta Mesons as Probes of the Hadronic Fireball in Nucleus-Nucleus Collisions around 1A GeV. Phys. Rev. C 67 024903.

Baran A, Broniowski W, Florkowski W (2004). Description of the Particle Ratios and Transverse-Momentum Spectra for Various Centralities at RHIC in a Single-Freeze-Out Model. Acta Physica Polonica B., 35: 779.

Becattini F, Cleymans J, Keranen A, Suhonen E, Redlich K (2001). Features of particle multiplicities and strangeness production in central heavy ion collisions between 1.7A and 158A GeV/c. Phys. Rev. C 64 024901.

Braun-Munzinger P, Redlich K, Stachel J (2004). nucl-th/0304013 and in Quark Gluon Plasma 3, eds. R.C. Hwa and X.N. Wang, (World Scientific Publishing, 2004).

Becattini F, Ga´zdzicki M, Ker¨anen A, Manninen J, Stock R (2004). Phys. Rev. C 69 024905. J. Manninen, F.Becattini and M. Ga´zdzicki, hep-ph/0511092.

Broniowski W, Florkowski W, Michalec M (2002). Thermal analysis of particle ratios and p_T spectra at RHIC. Acta Physica Polonica B Vol. 33: 761

Braun-Munzinger P, Stachel J, Wessels JP, Xu N (1995). Thermal Equilibration and Expansion in Nucleus-Nucleus Collision at the AGS. Phys. Lett. B 344 43 (1995) and Phys. Lett. B 365 1 (1996).

Braun-Munzinger P, Heppe I, Stachel J (1999). Chemical Equilibration in Pb+Pb Collisions at the SPS. Phys. Lett. B 465: 15.

Braun-Munzinger P, Magestro D, Redlich K, Stachel J (2002). Hadron production in Au-Au collisions at RHIC. Phys. Lett. B 518: 41.

Bravina L, Fuchs C, Faessler A, Zabrodin E (2002). Violation of energy-per-hadron scaling in resonance matter. Phys. Rev. C 66 014906.

By STAR Collaboration (2005). (J. Adams et al.). Experimental and Theoretical Challenges in the Search for the Quark Gluon Plasma: The STAR Collaboration's Critical Assessment of the Evidence from RHIC Collisions. Nucl.Phys. A 757 102.

Cleymans J, Satz H (1993). Thermal hadron production in high-energy heavy ion collisions. Z. Phys. C 57, 135-148.

Cleymans J, K¨ampfer B, Kaneta M, Wheaton S, Xu N (2005). Centrality dependence of thermal parameters deduced from hadron multiplicities in Au+Au collisions at$\sqrt{s_{NN}}$=130 GeV. Phys. Rev. C 71, 054901.

Cleymans J, Oeschler H, Redlich K (1999). Influence of Impact Parameter on Thermal Description of Relativistic Heavy Ion Collisions at GSI/SIS. Phys. Rev. C59 1663. K. Redlich and L. Turko, Z. Phys. C5 201 (1980).

Gosset J, Gutbrod HH, Meyer WG, Pokanger AM, Sandoval A, Stock R, Westfall GD (1977). Central collisions of relativistic heavy ions. Phys. Rev., C16, 629.

Hegab MK, Hussein MT, Hassan NM (1990). Nucleus - Nucleus Collisions at High Energies. Z. Phys. A 336, 345.

Hussein MT, Hassan NM, El-HARBY N (2000). Time Evolution of Fast Particles During the Decay of Hadronic Systems. Turk. J. Phy., 24: 501-511.

Kovchegov Y, Mueller AH (1998). Gluon production in current-nucleus and nucleon-nucleus collisions in a quasi-classical approximation. Nucl. Phys. B529 451; A.H. Mueller, hep-ph/ 9906322.

Kovner A, McLerran L, Weigert H (1998). Gluon Production at High Transverse Momentum in the McLerran-Venugopalan Model of Nuclear Structure Functions. Phys. Rev. D52, p. 3809 and 6231.

Kraus I (2005). Contribution to HEP2005, Europhysics Conference, Lisboa, Portugal, to be published in the proceedings of the conference.

McLerran L, Venugopalan R (1994). Gluon distribution functions for very large nuclei at small transverse momentum. Phys. Rev. D 49: 2233, 3352.

Proceedings of 14th Intern. Conference on Ultrarelativistic Nucleus-Nucleus Collisions (Quark Matter 99), Torino, Italy, (1999). Nucl. Phys. A661, 1c.